Cell

Structural Basis for Cooperativity in Recruitment of MAML Coactivators to Notch Transcription Complexes

Yunsun Nam,[1,4] Piotr Sliz,[2,4] Luyan Song,[3] Jon C. Aster,[3] and Stephen C. Blacklow[3,*]
[1] Biological and Biomedical Sciences Graduate Program in the Division of Medical Sciences, Harvard Medical School, Boston, MA 02115, USA
[2] Department of Biological Chemistry and Molecular Pharmacology, Harvard Medical School and Howard Hughes Medical Institute, 250 Longwood Ave., Boston, MA 02115, USA
[3] Department of Pathology, Brigham and Women's Hospital and Harvard Medical School, Boston, MA 02115, USA
[4] These authors contributed equally to this work.
*Contact: sblacklow@rics.bwh.harvard.edu
DOI 10.1016/j.cell.2005.12.037

SUMMARY

Notch receptors transduce essential developmental signals between neighboring cells by forming a complex that leads to transcription of target genes upon activation. We report here the crystal structure of a Notch transcriptional activation complex containing the ankyrin domain of human Notch1 (ANK), the transcription factor CSL on cognate DNA, and a polypeptide from the coactivator Mastermind-like-1 (MAML-1). Together, CSL and ANK create a groove to bind the MAML-1 polypeptide as a kinked, 70 Å helix. The composite binding surface likely restricts the recruitment of MAML proteins to promoters on which Notch:CSL complexes have been preassembled, ensuring tight transcriptional control of Notch target genes.

INTRODUCTION

Notch and its homologs define a unique class of highly conserved single-pass transmembrane receptors that anchor a metazoan signaling pathway that regulates cell growth, development, and death in a variety of tissues (Artavanis-Tsakonas et al., 1999). Genetic studies examining the role of Notch in different developmental contexts indicate that even small changes in the strength of Notch signals are sufficient to cause malformations and defects in tissue homeostasis. In addition, a variety of human pathologies result from mutations affecting certain of the four mammalian *NOTCH* receptors (*NOTCH1–4*) or their cognate ligands. For example, germline loss-of-function mutations in *NOTCH1* cause congenital aortic valve disease (Garg et al., 2005), mutations of *NOTCH3* result in an adult onset vasculopathy called CADASIL (Joutel et al., 1996), and loss-of-function mutations in the Notch ligand *JAGGED1* are found in Alagille syndrome, which is characterized by pleiotrophic developmental abnormalities (Li et al., 1997; Oda et al., 1997). Conversely, somatic gain-of-function mutations in *NOTCH1* occur in more than half of human T cell acute lymphoblastic leukemias (T-ALL; Ellisen et al., 1991; Weng et al., 2004), and other studies indicate that aberrations in Notch signaling can also contribute to neoplasia of the skin (Nicolas et al., 2003), breast (Uyttendaele et al., 1996), and gut (Fre et al., 2005; van Es et al., 2005).

Notch signaling is initiated when a ligand of the Delta, Serrate, and Lag-2 (DSL) family expressed on one cell binds to a Notch receptor on the surface of a neighboring cell (Fehon et al., 1990). Upon ligand stimulation, Notch undergoes regulated intramembrane proteolysis, which permits its intracellular portion (ICN) to translocate to the nucleus (De Strooper et al., 1999; Struhl and Grenwald, 1999; Ye et al., 1999). ICN then induces transcription of target genes by driving the assembly of a transcriptional activation complex that includes a DNA bound transcription factor called CSL (for *C*BF-1, suppressor of hairless, and *L*ag-1; Fortini and Artavanis-Tsakonas, 1994) and a coactivator protein of the Mastermind-like (MAML) family (Petcherski and Kimble, 2000a; Wu et al., 2000).

Genetic and biochemical studies have defined the regions of CSL, ICN, and MAML that are responsible for functional interactions of these proteins with one another. CSL is a highly conserved protein comprised of N-terminal and C-terminal Rel homology domains and a central β-trefoil domain that binds DNA in a sequence-specific fashion (Kovall and Hendrickson, 2004; Tun et al., 1994). Like other transcription factors that contain Rel homology domains (e.g., NF-κB), CSL activity is regulated by the formation of a complex with a protein partner (ICN) that contains a set of iterated ankyrin repeats (ANK). Although ICN can bind CSL with high affinity through an N-terminal domain called RAM, assembly of a functional transcriptional activation complex requires the presence of the ANK domain (Lubman et al., 2004; Rebay et al., 1993; Roehl et al., 1996;

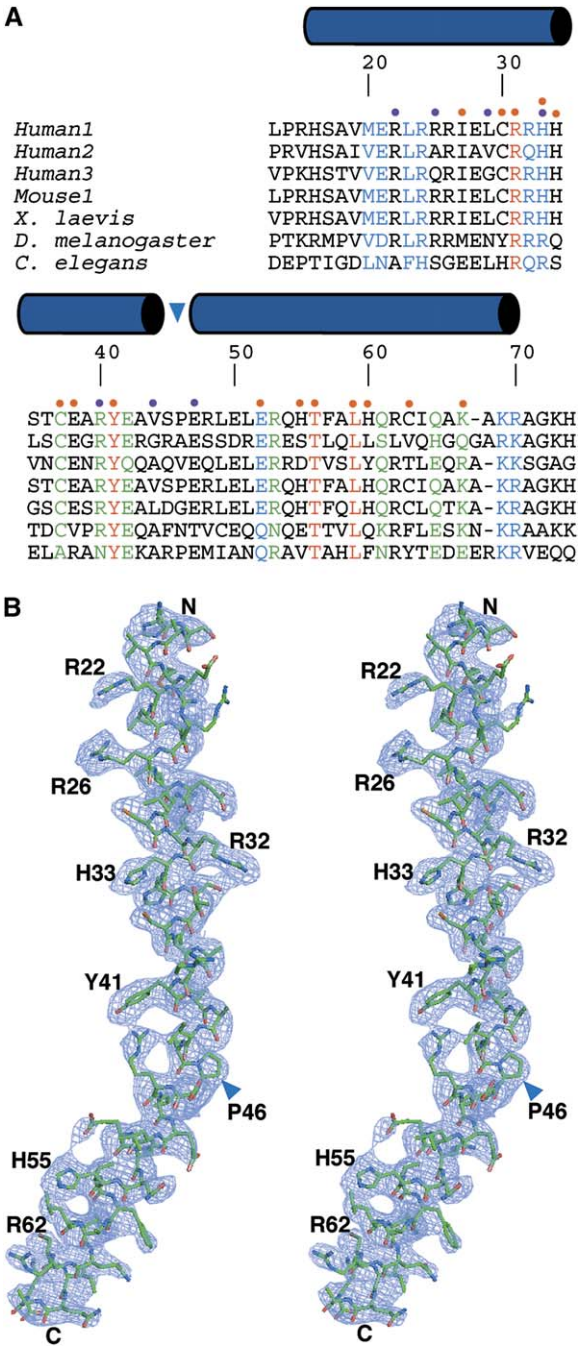

Figure 1. Sequence Alignment and Electron Density

(A) Sequence alignment. Residues 13-74 of human MAML-1 aligned with homologs from human (MAML-2 and MAML-3), mouse, *Drosophila melanogaster*, *Xenopus laevis*, and *Caenorhabditis elegans*. Helices are marked with cylinders above the sequence, and the kink in the helix is denoted with a blue arrow. Residues that are absolutely conserved are orange. Blue and green colors denote sites with conserved and semiconserved substitutions, respectively (ClustalW, http://www.ebi.ac.uk/clustalw/). Colored circles above the sequence denote residues that interact with ANK (purple) and/or CSL (orange).

(B) Electron density. View of a SigmaA-weighted composite omit map of the MAML-1:ANK:CSL:DNA complex contoured at 1σ after refinement to 3.25 Å resolution. Density around the MAML-1 polypeptide is shown. (B) and Figures 2–5 were generated using Pymol software (DeLano scientific; www.pymol.org). The coloring scheme for stick representation in all figures is as follows: carbon—ribbon color, green, yellow or gray; oxygen—red; nitrogen—blue; and sulfur—orange.

Roehl and Kimble, 1993), which also participates in CSL binding (Jarriault et al., 1995; Kodoyianni et al., 1992; Kurooka et al., 1998; Tani et al., 2001). Significantly, enforced expression of ICN proteins that have ANK but not RAM are capable of causing CSL-dependent Notch gain-of-function phenotypes (Aster et al., 2000; Jeffries et al., 2002; Roehl et al., 1996), indicating that the essential domain for the effector function of Notch at target promoters is ANK. The capacity of ANK to activate CSL-dependent transcription relies upon its ability to interact with a short 60–70 residue sequence at the N-terminal end of MAML (Figure 1A) that is sufficient for assembly of complexes that contain MAML, ICN, and CSL (Nam et al., 2003; Petcherski and Kimble, 2000a; Petcherski and Kimble, 2000b). Once the complex is assembled, the C-terminal portion of MAML not only contributes to transcriptional activation through association with p300, RNA polymerase II, and other unknown factors (Fryer et al., 2002; Wallberg et al., 2002), but also limits the longevity of the assembled complex by promoting the phosphorylation of ICN by CDK8, which leads to rapid ICN turnover (Fryer et al., 2004).

A central unanswered question in Notch signaling revolves around how ICN recruits MAML to ICN:CSL complexes. Remarkably, neither CSL nor the intracellular portion of Notch1 (ICN1) alone binds detectably to MAML-1, but together they cooperate to bind MAML-1 with high affinity (Nam et al., 2003; Petcherski and Kimble, 2000a; Petcherski and Kimble, 2000b), suggesting two possible recruitment mechanisms. First, binding of ANK to CSL could induce an allosteric change that creates a MAML binding site, a mechanism analogous to the manner in which steroid hormones induce conformational changes that make their receptors competent for coactivator loading (Nettles and Greene, 2005; Shiau et al., 1998). Alternatively, the association of ANK with CSL might create a novel composite binding site for MAML. To distinguish between these possibilities, we sought to solve structures of complexes consisting of the three critical protein components—ANK, CSL, and the N-terminal portion of MAML—assembled on cognate DNA.

RESULTS

We report here three structures determined by X-ray crystallography: two of complexes that contain the ANK domain of human ICN1, residues 13–74 of human MAML-1, and residues 9–435 of human CSL on different DNA duplexes, and a third of the ANK domain of human Notch1 solved to 1.55 Å resolution (Figures 1B and 2; Table 1 and Table S1 in the Supplemental Data available with this article online). One of the complexes, a MAML-1:ANK:CSL complex bound to an 18-mer blunt-ended DNA duplex from the HES-1 promoter, crystallized in

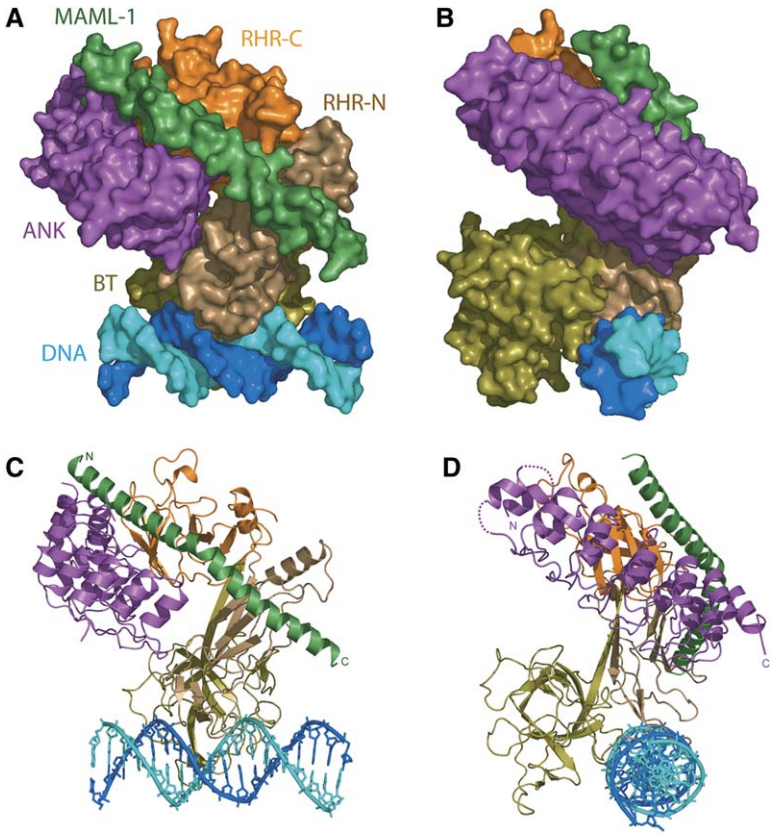

Figure 2. Overall Structure of the MAML-1:ANK:CSL:DNA Complex

(A and B) Molecular surface representation. (C and D) Ribbon representation. Two views related by a 90 degree rotation are shown. The ankyrin domain is colored purple; the MAML-1 polypeptide is colored dark green; and the RHR-N, β-trefoil, and RHR-C domains of CSL are colored light brown, gold, and orange, respectively. The two DNA strands are colored blue and cyan.

space group $P6_322$ and diffracted to 3.25 Å. The other complex, which was formed with a related 18-mer having a two-base overhang, stacked via a pseudocontinuous DNA helix in space group $P4_32_12$ and diffracted anisotropically between 4.3 and 7.5 Å. Despite different DNA sequences and different crystal packing interactions in the two complexes, there are no detectable differences in the relative positions of the proteins. All interactions described below are derived from the higher resolution structure with blunt-ended DNA.

Overview of the Structure of the MAML-1:ANK:CSL:DNA Complex

CSL and the ANK domain of Notch1 combine to create a binding groove that accommodates the MAML-1 polypeptide in a kinked helical conformation (Figures 2A and 2C). The N terminus of the MAML-1 polypeptide is located 60 Å from the DNA, but descends at an ~45 degree angle with respect to the DNA so that the last MAML-1 residue resolved in the structure approaches to within 15 Å of the penultimate phosphate group of the nearest DNA strand. Although the ANK domain and the MAML-1 polypeptide are themselves elongated, the complex is globular overall (~80 × 60 × 50 Å), with a cleft separating the DNA binding domain of CSL from the base of the ANK domain of Notch1 (Figures 2B and 2D).

The CSL protein in our complex has three domains, an N-terminal RHR-N domain, a DNA binding β-trefoil domain, and a C-terminal RHR-C domain (Figure 2). The extended overall arrangement among the three CSL domains does not change upon complexation with ANK and MAML-1 from that observed in the *Caenorhabditis elegans* CSL:DNA complex alone (Kovall and Hendrickson, 2004); the CSL proteins of the respective complexes superimpose with a backbone rmsd of 1.12 Å (Figure S1), and the interactions with DNA are preserved. The divergence between the two complexes is primarily restricted to two loops that are distant from both the partner proteins and the bound DNA, with crystal packing forces clearly responsible for the repositioning of one of them.

Our structure of the ANK domain from human Notch1 closely resembles the three other reported structures of partial (Lubman et al., 2005) or complete (Ehebauer et al., 2005; Zweifel et al., 2003) isolated Notch ANK domains (Figure S2). In each structure of an entire isolated Notch ANK domain including ours, repeats two through seven of the ANK domain adopt the characteristic ankyrin fold of two antiparallel α helices followed by a β hairpin or a long loop that projects roughly perpendicular to the long axis of the helical hairpin, whereas the first repeat is not resolved in the structure.

Both in isolation and in the complex, the consecutive ANK repeats stack together into an L-shaped domain, which curves to create a concave surface along the H1 helices. Repeats two through seven of the ANK domain associate with CSL as a rigid body, with little change in the

Table 1. Data Collection and Refinement Statistics

Crystal	ANK	CSL, SeMet ANK, MAML-1, Overhang DNA	CSL, SeMet ANK, MAML-1, Blunt-Ended DNA
Data Collection Statistics			
Space group	$P6_5$ (twinned)	$P4_32_12$	$P6_322$
Resolution range (Å)	30–1.55	25–4.3 (along a) or 7.5 (along b and c)	45–3.25
Molecules in asymmetric unit	2	1	1
Cell parameters (Å)	a = b = 97.93 c = 109.07	a = b = 107.5 c = 233.2	a = b = 273.9 c = 121.0
X-ray source	BNL NSLS X29A	BNL NSLS X29A	APS ANL19-ID
Mosaicity (°)	0.31	0.8	0.4
Number of unique reflections	85821	10505	79964
Multiplicity	2.2 (2.0)[a]	5.0 (5.1)[a]	3.6 (3.5)[a]
Completeness (%)	88.2 (45.9)[a]	93.8 (86.2)[a]	91.1 (89.3)[a]
R_{symm} (%)[b]	6.8 (37.5)[a]	9.0 (25.1)[a]	8.4 (41.1)[a]
$I/\sigma(I)$	11.9 (2.0)[a]	8.2 (2.63)[a]	19.7 (3.3)[a]
Refinement Statistics			
R_{free}(%)[c] (test set size/ count)	19.3 (5.5%/4762)	35.8 (4.7%/491)	25.7 (5.1%/3688)
R_{cryst}(%)[c]	15.7	35.8	22.2
Number of ANK atoms	1665 (A) and 1618 (B)	1660	1660
Number of CSL atoms	N/A	3370	3370
Number of MAML atoms	N/A	468	468
Number of DNA atoms	N/A	732	732
Number of water (W) and sulfate (S) atoms	414 (W) and 10 (S)	0	10 (W)
Average B (Å^2), average over all residues in each chain indicated	23.3 (chain A) 26.5 (chain B) 34.2 (solvent)	164.5 (overall B)	65.8 (ANK) 94.5 (CSL) 83.0 (MAML) 112.4 (DNA) 47.6 (solvent)
Rmsd bond length (Å)	0.005	0.010	0.010
Rmsd bond angle (°)	1.20	1.6	1.6
Rmsd dihedral (°)	20.6	22.7	22.7
Rmsd improper (°)	0.75	1.21	1.21
Ramachandron plot (%) (core, allowed, generous, dis-allowed)	87.1, 12.7, 0.3, 0.0	76.0, 21.9, 2.1, 0.0	76.0, 21.9, 2.1, 0.0
Estimated coordinate error from Luzzati plot (Å)	0.25	0.94	0.38

[a] Data for the outermost shell are given in parentheses.
[b] $R_{symm} = 100\ \Sigma\ |Ih - \langle Ih \rangle| / \Sigma\ Ih$, where $\langle Ih \rangle$ is the average intensity over symmetry equivalents.
[c] $R_{cryst/free} = 100\ \Sigma\ |F_o - F_c| / \Sigma |F_o|$. R_{cryst} and R_{free} were calculated from the working and test sets, respectively.

curvature of this part of the domain induced upon binding (Figure S2). The difference between the isolated ANK domain and the structure of ANK after complexation is that the first repeat acquires an ANK fold in the context of the complex. The induced folding of the first ANK repeat of Notch is likely to be general throughout the Notch family, as the residues that comprise the two helices are highly conserved, though the unstructured linker between them is not. Nevertheless, the first repeat is still more poorly ordered than the rest of the domain, with electron density evident only for the polypeptide backbone and certain bulky side chains on the two helices (helix H2 was modeled only as polyalanine). Indeed, truncated forms of ANK lacking the first repeat still form ternary complexes that are stable to gel filtration and even crystallize (data not shown). The N-terminal end of the ANK stack thus appears to be intrinsically more flexible than the C-terminal end of the stack, as previously suggested (Lubman et al., 2005). The N-terminal end of the first repeat also approaches the C-terminal end of CSL and the N-terminal end of MAML-1 in the complex, and its position might be more rigidly fixed in the context of the full-length proteins. Alternatively, it might be that the first repeat constitutes a recognition element that is induced after formation of this complex to recruit additional binding partners.

Features of the Interface between ANK and CSL

The ANK:CSL interface consists of two discontinuous contact sites (ANK:RHR-C and ANK:RHR-N), which together bury a total of 1040 Å^2 of solvent-accessible surface area on each protein (Figure 3). The groove created by the complex lies nearly parallel to the long axis of ANK along the interface with RHR-C, and the binding of MAML-1 in this groove further conceals the ANK:CSL interface from solvent. At the ANK:RHR-C site, the concave (inner) face of ANK interacts with the external-facing β sheet of RHR-C. The surface of ANK buried at this site corresponds roughly to that of IκB covered by the p65 RHR-C domain of the IκB:NFκB complex (Huxford et al., 1998; Jacobs and Harrison, 1998), though the detailed interactions between ANK and RHR-C as well as the relative positions of the RHR-N and -C domains differ when the ANK:CSL interface is compared with that of IκB:NFκB. At the ANK:RHR-N site, residues from the loops connecting ANK repeats five to six and six to seven come into contact with RHR-N. The contacts between the domains are capped at the ends by polar interactions that are largely conserved; the overall surface potential of the ANK domain at the interface is positive, in contrast to the region in contact with MAML-1, which is strongly negative (see below and Figure 4A).

Cooperative Binding of the Mastermind-like 1 Polypeptide as an Elongated Helix

The most striking feature of the structure is the elongated kinked helix adopted by residues 15–67 of the MAML-1 polypeptide and its interactions with ANK and CSL in the complex (Figure 4). A 40 degree kink around Pro 46 divides this 15 turn helix into two discrete N- and C-terminal parts. The N-terminal part is nestled in a groove at the ANK:RHR-C interface, bounded on one side by ANK and on the other by the RHR-C domain of CSL. A four-stranded β sheet of RHR-N perpendicular to the helix establishes a second, predominantly hydrophobic docking site exclusively on CSL for the C-terminal part of MAML-1 after the kink. On the ANK side, the N-terminal part of the MAML-1 helix rests on a concave ridge established by the H1-H2 loops of ANK repeats three through seven. Platforms at the two ends of the ridge serve as anchor points for interactions between ANK and this part of the helix (Figure 4B). At platform I (Figure 5A), which is highly acidic (Figure 4A), polar and charged interactions predominate among contacts between the H1-H2 loops of ANK repeats three and four and turns three and four of the MAML-1 helix. This platform ends with a hydrophobic interaction between MAML-1 L29 and ANK A2007. At platform II (Figure 5B), turns seven through nine of the MAML-1 helix interact with ANK repeats six and seven. Between the two platforms on ANK (Figure 4), the MAML-1 helix is suspended above the concavity in the ridge and rests against a bulge in the RHR-C domain of CSL (Figure 5C). Alternating hydrophobic and polar interactions make up the MAML-1:RHR-C interface and appear to guide the choice of helical register. The interface between the C-terminal part of the MAML-1 helix, and the four-stranded β sheet of RHR-N (Figure 5D) is centered around a hydrophobic patch on CSL and is capped at the C-terminal end by polar interactions.

DISCUSSION

Specificity in biological signaling often relies on motif recognition. Typical motifs are frequently 10 amino acids in length or fewer and routinely suffice to encode functional specificity in the cell. Transcriptional coactivation in hormone receptor signaling is no exception: the binding of hormones or small molecule agonists to nuclear hormone receptors recruits coactivators by inducing a conformational change in the hormone binding domain that uncovers a binding site for a short hydrophobic helical motif (Nettles and Greene, 2005; Shiau et al., 1998).

In contrast, neither Notch nor CSL undergoes a dramatic conformational change upon complexation, and therefore, MAML-1 detects a composite surface derived from both proteins, rather than of a smaller, allosterically induced binding site on CSL or ANK alone. As a result, the MAML-1 polypeptide "motif" in the Notch transcriptional activation complex includes a 52 residue helix, much longer than the typical recognition motif. Indeed, the 62-mer used here for crystallization is the shortest tested sequence that retains potent dominant-negative activity (Weng et al., 2003), blocking Notch signaling both in cells transfected with active forms of Notch, and in tumor cell lines with mutations in Notch1 that cause constitutively increased signaling (Weng et al., 2004). By recognizing parts of ANK and CSL at alternating surfaces along the long axis of the ANK:CSL protein-protein interface, MAML-1

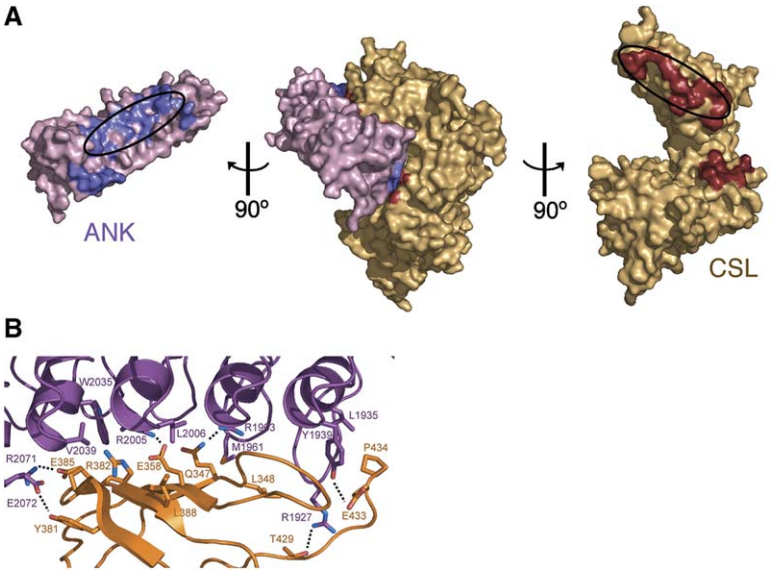

Figure 3. Interactions between ANK and RHR-C

(A) Molecular surface representation. Center panel: the ANK domain of Notch1 is pink, and CSL is beige. Left panel: the ANK domain has been rotated clockwise, and residues that approach within 4 Å of CSL are colored slate-blue. Right panel: CSL has been rotated counterclockwise and residues that approach within 4 Å of ANK are colored crimson. MAML-1 and DNA have been removed for clarity. Ovals denote the regions of ANK and RHR-C at the interface in (B).

(B) Details of the ANK-RHR-C interface. The backbone of ANK is a purple ribbon, with side chains that approach within 4 Å of RHR-C rendered as sticks. The backbone of RHR-C is an orange ribbon, with side chains that approach within 4 Å of ANK rendered as sticks. Side chain hydrogen bonds are indicated with dotted black lines. Residues from ANK at the interface with RHR-C include side chains projecting from the H1 helices that line the concave surface of the domain, as well as additional residues from the repeat one through two and repeat two through three loops. Polar interactions help to cap the interactions between the N-terminal end of ANK and RHR-C, and they are likely to be important in fixing the positions of the two domains with respect to each other. Near the N-terminal end of ANK and the C-terminal end of RHR-C, side chain hydrogen bonds are formed between the following pairs of residues: ANK R1927 and the side chain hydroxyl of T429 from RHR-C, ANK Y1939 and E433 of RHR-C. Moving along the ankyrin repeat stack, additional side chain hydrogen bonds are formed between ANK R1963 and Q347 of CSL, ANK R2005 and CSL E358, ANK R2071 and CSL E385, and ANK E2072 and CSL Y381. There are also hydrophobic interactions along the interface: among ANK L1935, ANK Y1939, and RHR-C P434, between ANK M1961 and CSL L348, between ANK L2006 and CSL L388, and around ANK W2035, which contacts the methyl group of T360 and the aliphatic portion of E385 from CSL. Adjacent to W2035, A2038 and V2039 of ANK come into contact with the aliphatic parts of R382 and C383 from CSL.

At the secondary docking site (not shown), there is a cluster of interactions that includes contacts from the side chains of H2093 and M2094 from ANK with the side chains of H124 and M126 from RHR-C. Polar interactions that cap this site at the C-terminal end of ANK include contacts between the imidazole ring of ANK H2093 with the guanidino group of CSL R146, between the carboxylate of ANK D2095 and the backbone amide of CSL K123, and between the guanidino group of ANK R2096 and the CSL N93 side chain amide.

ensures binding to the Notch:CSL complex with high affinity, in the absence of tight binding to either protein alone. Further stringency in recognition is achieved by requiring the MAML-1 sequence to fold into a relatively rigid helical conformation to form a productive complex, because the MAML-1 polypeptide is not folded until bound (Figure S5).

Though MAML-1 is less well conserved than either CSL or the ANK domain of Notch, the sequence variability in MAML-1 occurs primarily at positions on the exposed face of the helix not in contact with ANK or CSL. In fact, four of the seven residues that interact with ANK are identical among all three human MAML proteins, as are all eight of the MAML residues that contact the RHR-C domain of CSL (Figure 1A). Although all three mammalian MAML proteins form complexes with ICN1 and CSL, reporter-gene assays suggest that the relative coactivation strength of MAML-1, MAML-2, and MAML-3 varies, with MAML-1 and MAML-2 being more potent coactivators for ICN1 than MAML-3 (Wu et al., 2002). Further work will be needed to determine whether these functional differences stem from sequence variation in the CSL and ANK binding region, from differences in posttranslational modifications that differentially regulate the affinity of the N-terminal regions for Notch:CSL complexes, or from effects due to the less well-conserved C-terminal parts of the MAML proteins. More generally, several key MAML-1 residues buried in the interface with CSL—Y41, T56, L59, and R62—are absolutely conserved among all species (Figure 1A). The most divergent sequence belongs to the *C. elegans* MAML protein LAG-3, which lacks an otherwise conserved arginine-rich sequence (RLRRR) tethering the N-terminal end of MAML-1 to ANK in our structure. Strikingly, the sequences of the ANK domains of the worm proteins also diverge at the positions in contact with the MAML-1 N terminus: D1973 of human Notch1 is replaced by a positively charged residue in both LIN-12 and GLP-1, and E2009 of human Notch1 is located at the site of an ~10 residue insertion in both worm Notch proteins. These correlated changes of LAG-3 and the ANK domains appear to represent covariation needed to maintain a binding interface, and the species differences at these sites probably explain the observed failure of cross-species complexes to form when worm LAG-3 and either murine or fly components are mixed (Petcherski and Kimble, 2000b).

Mutational studies of the ANK domains of various Notch proteins have implicated residues from ANK repeats two, four, five, and seven as important for proper function (Lubman et al., 2004). Phenotypically identified mutations, which include a CADASIL mutation of human Notch3 in the H1-H2 loop of ANK repeat two and a hypomorphic

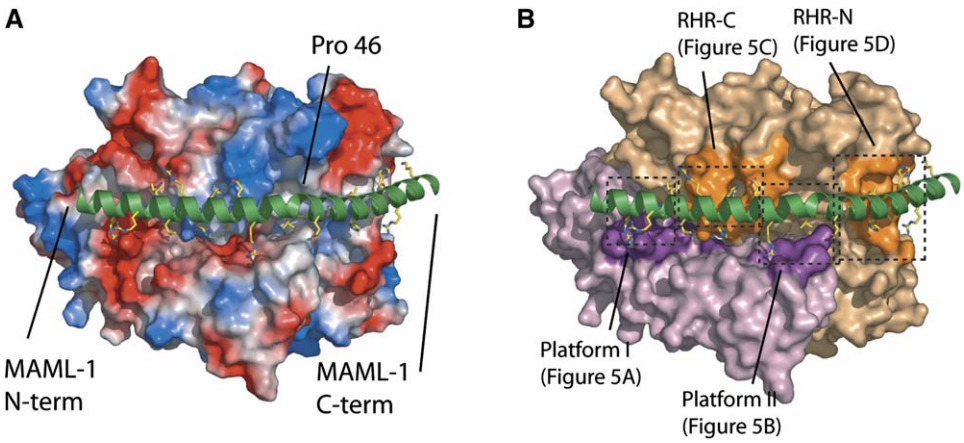

Figure 4. Cooperative Binding of MAML-1 by ANK and CSL

The MAML-1 helix is rendered as a green helical ribbon with side chains that approach within 4 Å of either ANK or CSL shown as sticks.

(A) The surfaces of ANK and CSL colored according to vacuum electrostatic potential on a sliding scale from red (−75 kT) to white (0 kT) to blue (75 kT).

(B) Sites where MAML-1 contacts ANK and CSL. The surface of ANK is colored dark purple where an atom of MAML-1 approaches within 4 Å and light purple elsewhere. The surface of CSL is colored dark orange where an atom of MAML-1 approaches within 4 Å and light orange elsewhere.

mutant of *Drosophila* Notch (called Su42c and equivalent to a V2039A substitution on H1 of human ANK repeat five) are located at positions in contact with MAML-1 and CSL, respectively. In contrast, multiresidue substitutions in ANK repeats four or seven predicted (Lubman et al., 2004) or shown (Zweifel et al., 2003) to unfold the ANK domain or dramatically reduce its stability do not alter residues in direct contact with either CSL or MAML-1, suggesting that these mutations compromise function indirectly by disrupting ANK structure around platforms I and II, respectively.

Functional Implications for Transcriptional Activation

Before Notch is proteolytically released from the membrane in its active form, CSL is in a complex with corepressor proteins at target DNA sites. Based on mutational studies, these corepressor proteins, which include SMRT (silencing mediator of retinoid and thyroid receptors)/N-coR (nuclear repressor corepressor) and CIR (CBF-1-interacting repressor), appear to bind directly to the β-trefoil domain of CSL (Hsieh et al., 1999; Kao et al., 1998). The corepressor binding site partially overlaps the proposed binding site on CSL for RAM (Kovall and Hendrickson, 2004) but is distant from the ANK binding site, which lies entirely within the Rel-homology region (Figures 2 and 3). Whether the conversion of CSL from a repressor into an activator results from direct displacement of corepressors thus remains an open question, especially because enforced expression of intracellular Notch variants lacking the RAM domain can still turn on CSL-dependent transcription and confer Notch gain-of-function phenotypes (Aster et al., 2000; Jeffries et al., 2002; Roehl et al., 1996).

Our structure, taken together with previous biochemical studies, supports a model in which the assembly of the Notch transcriptional activation complex occurs in a series of distinct steps (Figure 6). After translocation into the nucleus, Notch must first be delivered to CSL on DNA. Physiologic Notch signaling may rely on the natively unstructured region adjacent to the ANK domain called RAM, which has high affinity for the β-trefoil domain of CSL, to achieve this step (though variants of Notch lacking the RAM domain can transduce signals and even suffice to induce T-ALL in mouse models when expressed at high levels, as noted above [Aster et al., 2000]). After the recruitment step, ANK docks onto the Rel-homology region of CSL to create the composite surface recognized by the MAML-1 helix.

Transcriptional activation by nuclear Notch complexes then appears to depend on the use of p300 to connect Notch to the transcription machinery, but the molecular basis for recruitment of p300 to Notch:CSL complexes has been controversial. On the one hand, it has been contended that a region corresponding to the seventh ankyrin repeat of ICN1 links Notch:CSL complexes to the transcriptional machinery by directly binding to p300 (Oswald et al., 2001). On the other hand, studies by two different groups have reported that p300 binds to MAML-1 directly and that Notch:CSL complexes cannot bring p300 to DNA in cell-free systems, arguing that the role of Notch in recruiting p300 is indirect (Fryer et al., 2002; Wallberg et al., 2002). The structure of the complex reported here shows that the seventh ankyrin repeat of Notch is engaged in crucial interactions with MAML-1 at the epicenter of the complex right in the neighborhood of the kink in the helix, and it is unlikely that this ankyrin repeat would also be capable of directly binding to p300. Therefore, our data lend support to the model in which recruitment of p300 by ICN is indirect as a result of its interactions with MAML, a conclusion also reached by consideration of the deleterious effects on ANK domain stability likely to occur from the

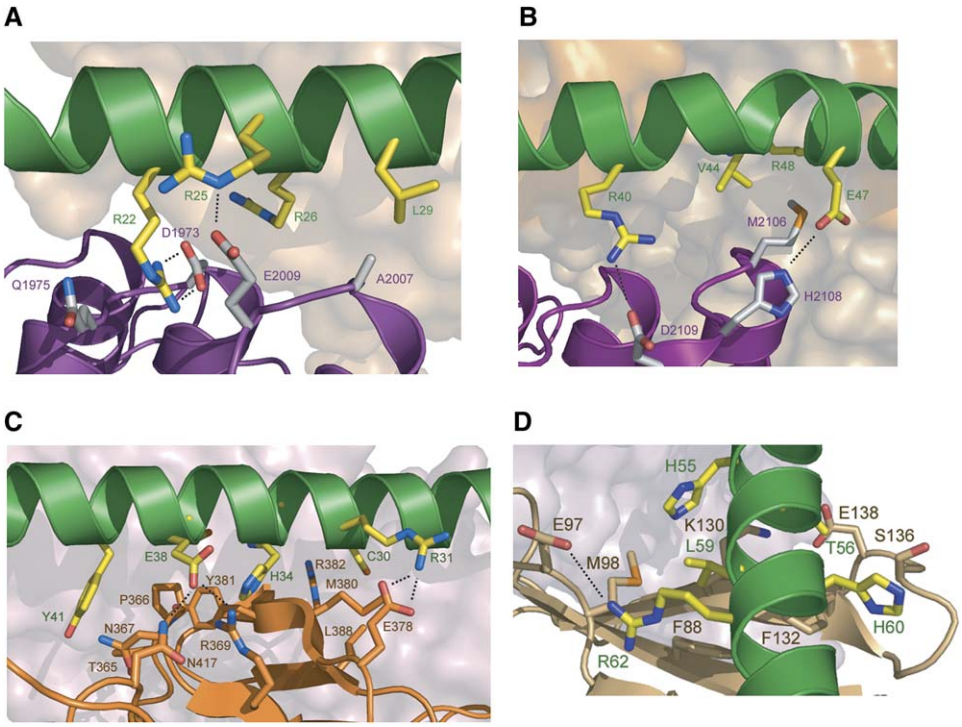

Figure 5. MAML-1 Binding Interfaces

(A and B) Interactions with ANK.

(A) Platform I interactions. Contacts include a salt-bridge between MAML-1 R22 and ANK D1973, hydrogen bonds from the MAML-1 R22 side chain to ANK Q1975 and to the backbone carbonyl oxygen of ANK E2009, and a salt bridge between MAML-1 R25 and ANK E2009.

(B) Platform II interactions. The guanidino group of MAML-1 R40 forms H bonds with the carboxylate of ANK D2109, and M2106 from ANK repeat seven at the tip of the platform has hydrophobic interactions with MAML-1 V44 and with the aliphatic portions of E47 and R48. The backbone of ANK is a purple ribbon, with side chains that approach within 4 Å of MAML-1 rendered as sticks. The MAML-1 helix is rendered as a green helical ribbon with side chains that approach within 4 Å of ANK shown as sticks.

(C and D) Interactions with CSL.

(C) RHR-C interactions. The first hydrophobic cluster includes I27, C30, and the aliphatic portion of R31 from turns five and six of the MAML-1 helix and M356, M380, and L388 of the CSL RHR-C domain. A salt bridge between R31 of MAML-1 and E378 of CSL anchors an adjacent set of polar interactions, which also include buried hydrogen bonds between H33 and H34 and the backbone carbonyl groups of CSL residues R382 and P366, respectively, a second salt bridge between MAML-1 E38 and CSL R369, and a hydrogen bond between E38 and the side chain amide of CSL N417. Hydrophobic interactions among the aliphatic part of MAML-1 E38, MAML-1 Y41, and the aliphatic parts of CSL T365, P366, and N367 complete the MAML-1:RHR-C interface.

(D) RHR-N interactions. CSL residues F88, M98, F132, and the aliphatic part of K130 contact the nonpolar parts of side chains from two consecutive turns of the MAML-1 helix: H55, the methyl group of T56, L59, and H60. Polar interactions at the C-terminal part of MAML-1 include contacts between the side chain of MAML-1 R62 and the side chain of CSL E97, and between the sulfhydryls of MAML-1 C63 and CSL C86. Side chain nitrogen atoms from R53, H60, and R62 of MAML-1 also form hydrogen bonds to the backbone carbonyl groups of S136, G134, and M98 of CSL, respectively. The backbone of CSL is an orange ribbon, with side chains that approach within 4 Å of MAML-1 rendered as sticks. The MAML-1 helix is rendered as a green helical ribbon with side chains that approach within 4 Å of CSL shown as sticks.

repeat seven mutations used to probe p300 recruitment (Lubman et al., 2004). Whether MAML-1 is preassociated with other components of the transcriptional machinery, such as p300 and CyclinC:CDK8:RNA polymerase II, or these components are recruited via MAML-1 subsequent to complex assembly remains to be determined. The recruitment of Cyclin C:CDK8 complex has been suggested to couple transcriptional activation with the disassembly and destruction of the ternary complex (Fryer et al., 2004); given the stability of the isolated complex, these steps are also likely to proceed through a series of tightly regulated events.

EXPERIMENTAL PROCEDURES

Protein and DNA Purification

MAML-1 13–74 and the ANK domain (residues 1873–2127) of human Notch1 were purified as previously described (Nam et al., 2003). For selenomethionine derivatives, the same expression vector and cells were used but were cultured to induce feedback inhibition of methionine biosynthesis by adding amino acids to minimal media immediately before induction. Human CSL (residues 9–435) was expressed with a C-terminal hexahistidine tag in *Escherichia coli* strain BL21 (DE3) pLysS (Stratagene) using a pET28a vector (Novagen). The culture was grown at 18°C, induced at OD600 = 0.8 with 0.5 mM IPTG, and cells were harvested 14 hr after induction. Cell pellets were lysed in buffer A (50 mM Tris [pH 8.8], 500 mM NaCl, 5 mM β-mercaptoethanol)

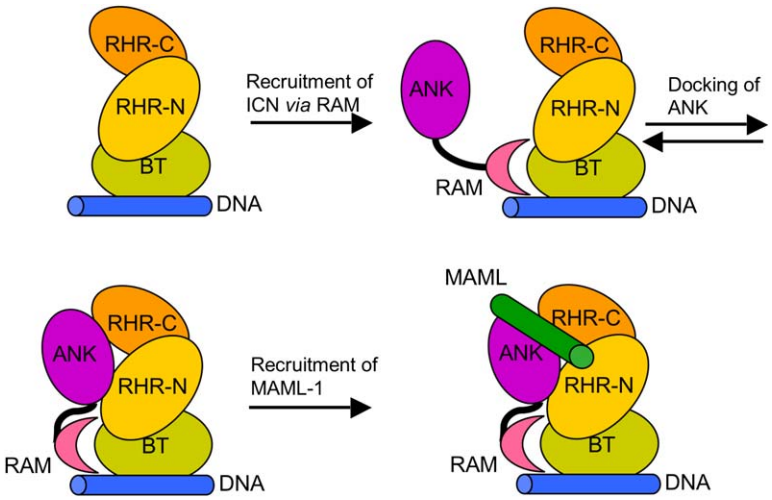

Figure 6. Model for Stepwise Assembly of the Core of the Notch Transcriptional Activation Complex

Intracellular Notch is initially recruited to the CSL:DNA complex by the RAM sequence of ICN, which has high affinity for the β-trefoil domain of CSL. The ANK domain of ICN then docks against the Rel-homology portion of CSL to create a high-affinity binding site for MAML-1. In the model, transient association of ANK with the Rel-homology domain of CSL (indicated as a reversible step) becomes clamped by MAML-1 binding.

by sonication, the lysate was cleared of insoluble matter by centrifugation and loaded onto Ni-NTA resin (Qiagen). The protein was eluted with 200 mM imidazole in buffer A, then further purified by anion-exchange chromatography on a MonoQ HR 10/10 column (Amersham Biosciences) in buffer B (20 mM Tris 8.8, 5 mM DTT), using a 100–500 mM NaCl gradient for elution. Complexes of CSL, ANK, and MAML-1 polypeptides were mixed at approximately 1:1:1 stoichiometry and purified away from uncomplexed polypeptides by gel filtration on a Superdex 200 column (Amersham Biosciences) in buffer C (20 mM Tris 8.5, 150 mM NaCl, 5 mM DTT). Oligonucleotides were purified by anion-exchange chromatography (BioscaleQ10, Biorad) and annealed in TE buffer. The DNA sequences were: 5′-GTTACTGTGGGAAAGAAA-3′ and 5′-TTTCTTTCCCACAGTAAC-3′ in the blunt-ended duplex and 5′-AGTTACTGTGGGAAAGAA-3′ and 5′-CTTTCTTTCCCACAGTAA-3′ in the two-base overhanging duplex.

Data Collection

All data were collected at 12.659 kEv (the peak energy of selenium) and processed with HKL2000 (Otwinowski and Minor, 1997). Data collection details and final refinement statistics for all three structures are presented below and in Tables 1 and S1.

Crystallization and Structure Determination

Isolated ANK Domain ($P6_5$ Crystals with Merohedral Twinning)

Crystals of the isolated ANK domain grew from hanging drops 24–72 hr after the protein solution (10 mg/ml, in 20 mM Tris [pH 8.5], 150 mM NaCl, 5 mM DTT) was mixed with an equal volume of reservoir solution (100 mM Tris [pH 8.5] and 1M ammonium sulfate). Crystals were cryoprotected by soaking in mother liquor with 20% glycerol and flash-frozen in liquid nitrogen prior to data collection. A native data set was collected at beamline X29A at Brookhaven National Laboratory, and the structure was solved by molecular replacement with MOLREP (Vagin and Teplyakov, 1997), using the *Drosophila* ankyrin repeat structure (1OT8; Zweifel et al., 2003) as a search model. Model building and refinement were done with ARP/wARP (Perrakis et al., 1997), REFMAC5 (Vagin et al., 2004), and COOT (Emsley and Cowtan, 2004). The twinning fraction was calculated by CNS to be 33%, which was then used for subsequent steps in CNS refinement algorithms for twinned data (Brunger et al., 1998).

Overhanging DNA Complex ($P4_32_12$ Crystals)

Protein-DNA complexes (5 mg/ml) formed with CSL, selenomethionine-derivatized ANK, MAML-1, and overhang DNA crystallized from hanging drops ~24 hr after mixing with an equal volume of reservoir solution (60 mM sodium citrate [pH 5.0], 2% PEG 8000, and 10% xylitol). Crystals were briefly soaked in 30 mM sodium citrate (pH 5.0), 50 mM NaCl, and 25% xylitol before freezing in liquid nitrogen prior to data collection at Brookhaven National Laboratory (beamline X29A). The crystals diffracted anisotropically to 4.3 Å along the c axis that runs parallel to the DNA stack and to 7.5 Å along axes a and b. The structure of the complex was determined by molecular replacement in MOLREP using the structure of worm CSL on DNA (Kovall and Hendrickson, 2004) and our human ANK structure as search models. Anomalous Fourier difference maps showed agreement between ANK's selenium peaks and the methionine sites in ANK as positioned by molecular replacement.

After rigid body refinement in CNS, a long tube of curved helical density corresponding to MAML-1 became apparent and was initially modeled without an assigned helix orientation using a 26 residue helix kinked in the middle by a proline (PDB code 1D8C, chain A, residues 32–70). Other long helices with proline in the middle fit equally well. Using the combinatorial extension (CE) method (http://cl.sdsc.edu/), we identified ten more such helices all with an average bend angle of 40 degrees. Subsequently, the helical model was confirmed and its orientation was determined by Se-Met scanning of MAML-1. Briefly, single methionines were introduced in place of L29, V44, L49, L51, or L59 of MAML-1 to make five Se-Met derivatized MAML-1 polypeptides, which were then crystallized in complexes. The anomalous signal resulting from each introduced methionine mutation was used to define the orientation and register of the MAML-1 helix (Table S1; Figure S4). After placing the kinked helix model of MAML-1 according to the Se-Met scanning results, CNS rigid body refinement was used to refine the position of the kinked helix. For final refinement, the structure of the blunt-ended DNA complex (determined as described below) was used as a starting model for rigid body refinement, and the MAML-1 register in the resulting model remained consistent with the Se-Met scanning results from the $P4_32_12$ crystals.

Blunt-Ended DNA Complex ($P6_322$ Crystals)

Complexes with the blunt-ended DNA duplex were assembled essentially as for the complexes described above, also using Se-Met ANK. Crystals grew from hanging drops containing equal volumes of protein (5 mg/ml)/DNA solution and reservoir buffer (50 mM HEPES [pH 7.9], 6% PEG 3350, and 5% ethylene glycol). Crystals were cryoprotected by soaking in mother liquor supplemented with ethylene glycol (25%) for flash-freezing in liquid nitrogen. The data set was collected at beamline 19ID of the Structural Biology Center at Argonne National Laboratory. Molecular replacement using MOLREP resulted in identical solutions when either the *C. elegans* CSL structure or our model from the $P4_32_12$ crystals was used as the search model. Model building and refinement were accomplished through iterative cycles of simulated annealing (CNS), group B factor refinement and modeling using O (Jones et al., 1991) as well as COOT (Emsley and Cowtan, 2004). In these

cycles, we included restraints for secondary structure (helices) and DNA conformation, and sharpened maps were used to aid with model building. The final model includes residues 11–434 of CSL, residues 1884–1892 and 1920–2120 of ANK, residues 16–70 of MAML-1, and all 18 nucleotides of each DNA strand. Helical density corresponding to helix H2 from the first ANK repeat was modeled as polyalanine due to weak side chain electron density in that region. Peaks above 3 sigma in the $F_o - F_c$ map with a shape resembling water were identified and initially populated with water molecules. After one refinement step, peaks with fewer than two hydrogen-bonding interactions or a B factor above 80 $Å^2$ were rejected, leaving ten water molecules present in the final model.

Although there is only one complex in each asymmetric unit, the ANK subunit of one complex makes crystal contacts with the ANK subunit of an adjacent complex. These contacts include the following interactions: residues K1946 and E1950 of one ANK subunit form salt bridges with E1950 and K1946 of the interacting subunit and R1985 of each ANK subunit contacts several backbone carbonyl groups of the adjacent ANK subunit. Although these interactions are crystal contacts that hold the lattice together, the identical interactions are also present in the structure of ANK determined separately at higher resolution.

Supplemental Data

Supplemental Data include five figures and one table and can be found with this article online at http://www.cell.com/cgi/content/full/124/5/973/DC1/.

ACKNOWLEDGMENTS

We thank Dr. Michael J. Eck and Dr. Stephen C. Harrison for helpful discussions, sharing facilities, and critical review of the manuscript. We are grateful to Deborah Kelly and Tom Walz for evaluating the quality of protein complexes by electron microscopy. This work was supported by NIH grants CA92433 and CA119130 (to S.C.B.) and the HHMI (P.S.). Use of the Argonne National Laboratory Structural Biology Center beamline 19ID was supported by the US Department of Energy (DOE) and of the Brookhaven National Laboratory beamline X29A by DOE and NIH.

Received: September 20, 2005
Revised: November 1, 2005
Accepted: December 12, 2005
Published: March 9, 2006

REFERENCES

Artavanis-Tsakonas, S., Rand, M.D., and Lake, R.J. (1999). Notch signaling: cell fate control and signal integration in development. Science *284*, 770–776.

Aster, J.C., Xu, L., Karnell, F.G., Patriub, V., Pui, J.C., and Pear, W.S. (2000). Essential roles for ankyrin repeat and transactivation domains in induction of T-cell leukemia by notch1. Mol. Cell. Biol. *20*, 7505–7515.

Brunger, A.T., Adams, P.D., Clore, G.M., DeLano, W.L., Gros, P., Grosse-Kunstleve, R.W., Jiang, J.S., Kuszewski, J., Nilges, M., Pannu, N.S., et al. (1998). Crystallography & NMR system: a new software suite for macromolecular structure determination. Acta Crystallogr. D Biol. Crystallogr. *54*, 905–921.

De Strooper, B., Annaert, W., Cupers, P., Saftig, P., Craessaerts, K., Mumm, J.S., Schroeter, E.H., Schrijvers, V., Wolfe, M.S., Ray, W.J., et al. (1999). A presenilin-1-dependent gamma-secretase-like protease mediates release of Notch intracellular domain. Nature *398*, 518–522.

Ehebauer, M.T., Chirgadze, D.Y., Hayward, P., Martinez Arias, A., and Blundell, T.L. (2005). High-resolution crystal structure of the human Notch 1 ankyrin domain. Biochem. J. *392*, 13–20.

Ellisen, L.W., Bird, J., West, D.C., Soreng, A.L., Reynolds, T.C., Smith, S.D., and Sklar, J. (1991). TAN-1, the human homolog of the *Drosophila* notch gene, is broken by chromosomal translocations in T lymphoblastic neoplasms. Cell *66*, 649–661.

Emsley, P., and Cowtan, K. (2004). Coot: model-building tools for molecular graphics. Acta Crystallogr. D Biol. Crystallogr. *60*, 2126–2132.

Fehon, R.G., Kooh, P.J., Rebay, L., Regan, C.L., Xu, T., Muskavitch, M.A.T., and Atravanis-Tsakonas, S. (1990). Molecular interactions between the protein products of the neurogenic loci *Notch* and *Delta*, two EGF-homologous genes in *Drosophila*. Cell *61*, 523–534.

Fortini, M.E., and Artavanis-Tsakonas, S. (1994). The suppressor of hairless protein participates in notch receptor signaling. Cell *79*, 273–282.

Fre, S., Huyghe, M., Mourikis, P., Robine, S., Louvard, D., and Artavanis-Tsakonas, S. (2005). Notch signals control the fate of immature progenitor cells in the intestine. Nature *435*, 964–968.

Fryer, C.J., Lamar, E., Turbachova, I., Kintner, C., and Jones, K.A. (2002). Mastermind mediates chromatin-specific transcription and turnover of the Notch enhancer complex. Genes Dev. *16*, 1397–1411.

Fryer, C.J., White, J.B., and Jones, K.A. (2004). Mastermind recruits CycC:CDK8 to phosphorylate the Notch ICD and coordinate activation with turnover. Mol. Cell *16*, 509–520.

Garg, V., Muth, A.N., Ransom, J.F., Schluterman, M.K., Barnes, R., King, I.N., Grossfeld, P.D., and Srivastava, D. (2005). Mutations in NOTCH1 cause aortic valve disease. Nature *437*, 270–274.

Hsieh, J.J., Zhou, S., Chen, L., Young, D.B., and Hayward, S.D. (1999). CIR, a corepressor linking the DNA binding factor CBF1 to the histone deacetylase complex. Proc. Natl. Acad. Sci. USA *96*, 23–28.

Huxford, T., Huang, D.B., Malek, S., and Ghosh, G. (1998). The crystal structure of the IκBα/NF-κB complex reveals mechanisms of NF-κB inactivation. Cell *95*, 759–770.

Jacobs, M.D., and Harrison, S.C. (1998). Structure of an IκBα/NF-κB complex. Cell *95*, 749–758.

Jarriault, S., Brou, C., Logeat, F., Schroeter, E.H., Kopan, R., and Israel, A. (1995). Signalling downstream of activated mammalian Notch. Nature *377*, 355–358.

Jeffries, S., Robbins, D.J., and Capobianco, A.J. (2002). Characterization of a high-molecular-weight Notch complex in the nucleus of Notch(ic)-transformed RKE cells and in a human T-cell leukemia cell line. Mol. Cell. Biol. *22*, 3927–3941.

Jones, T.A., Zou, J.Y., Cowan, S.W., and Kjeldgaard, M. (1991). Improved methods for building protein models in electron density maps and the location of errors in these models. Acta Crystallogr. A *47*, 110–119.

Joutel, A., Corpechot, C., Ducros, A., Vahedi, K., Chabriat, H., Mouton, P., Alamowitch, S., Domenga, V., Cecillion, M., Marechal, E., et al. (1996). Notch3 mutations in CADASIL, a hereditary adult-onset condition causing stroke and dementia. Nature *383*, 707–710.

Kao, H.Y., Ordentlich, P., Koyano-Nakagawa, N., Tang, Z., Downes, M., Kintner, C.R., Evans, R.M., and Kadesch, T. (1998). A histone deacetylase corepressor complex regulates the Notch signal transduction pathway. Genes Dev. *12*, 2269–2277.

Kodoyianni, V., Maine, E.M., and Kimble, J. (1992). Molecular basis of loss-of-function mutations in the glp-1 gene of Caenorhabditis elegans. Mol. Biol. Cell *3*, 1199–1213.

Kovall, R.A., and Hendrickson, W.A. (2004). Crystal structure of the nuclear effector of Notch signaling, CSL, bound to DNA. EMBO J. *23*, 3441–3451.

Kurooka, H., Kuroda, K., and Honjo, T. (1998). Roles of the ankyrin repeats and C-terminal region of the mouse notch1 intracellular region. Nucleic Acids Res. *26*, 5448–5455.

Li, L., Krantz, I.D., Deng, Y., Genin, A., Banta, A.B., Collins, C.C., Qi, M., Trask, B.J., Kuo, W.L., Cochran, J., et al. (1997). Alagille syndrome

is caused by mutations in human Jagged1, which encodes a ligand for Notch1. Nat. Genet. *16*, 243–251.

Lubman, O.Y., Korolev, S.V., and Kopan, R. (2004). Anchoring notch genetics and biochemistry: Structural analysis of the ankyrin domain sheds light on existing data. Mol. Cell *13*, 619–626.

Lubman, O.Y., Kopan, R., Waksman, G., and Korolev, S. (2005). The crystal structure of a partial mouse Notch-1 ankyrin domain: repeats 4 through 7 preserve an ankyrin fold. Protein Sci. *14*, 1274–1281.

Nam, Y., Weng, A.P., Aster, J.C., and Blacklow, S.C. (2003). Structural requirements for assembly of the CSL.intracellular Notch1.Mastermind-like 1 transcriptional activation complex. J. Biol. Chem. *278*, 21232–21239.

Nettles, K.W., and Greene, G.L. (2005). Ligand control of coregulator recruitment to nuclear receptors. Annu. Rev. Physiol. *67*, 309–333.

Nicolas, M., Wolfer, A., Raj, K., Kummer, J.A., Mill, P., van Noort, M., Hui, C.C., Clevers, H., Dotto, G.P., and Radtke, F. (2003). Notch1 functions as a tumor suppressor in mouse skin. Nat. Genet. *33*, 416–421.

Oda, T., Elkahloun, A.G., Pike, B.L., Okajima, K., Krantz, I.D., Genin, A., Piccoli, D.A., Meltzer, P.S., Spinner, N.B., Collins, F.S., and Chandrasekharappa, S.C. (1997). Mutations in the human Jagged1 gene are responsible for Alagille syndrome. Nat. Genet. *16*, 235–242.

Oswald, F., Tauber, B., Dobner, T., Bourteele, S., Kostezka, U., Adler, G., Liptay, S., and Schmid, R.M. (2001). p300 Acts as a transcriptional coactivator for mammalian notch-1. Mol. Cell. Biol. *21*, 7761–7774.

Otwinowski, Z., and Minor, W. (1997). Processing of X-ray diffraction data collected in oscillation mode. Methods Enzymol. *276*, 307–326.

Perrakis, A., Sixma, T.K., Wilson, K.S., and Lamzin, V.S. (1997). wARP: improvement and extension of crystallographic phases by weighted averaging of multiple-refined dummy atomic models. Acta Crystallogr. D Biol. Crystallogr. *53*, 448–455.

Petcherski, A.G., and Kimble, J. (2000a). LAG-3 is a putative transcriptional activator in the C. elegans Notch pathway. Nature *405*, 364–368.

Petcherski, A.G., and Kimble, J. (2000b). Mastermind is a putative activator for Notch. Curr. Biol. *10*, R471–R473.

Rebay, I., Fehon, R.G., and Artavanis-Tsakonas, S. (1993). Specific truncations of *Drosophila* Notch define dominant activated and dominant negative forms of the receptor. Cell *74*, 319–329.

Roehl, H., and Kimble, J. (1993). Control of cell fate in C. elegans by a GLP-1 peptide consisting primarily of ankyrin repeats. Nature *364*, 632–635.

Roehl, H., Bosenberg, M., Blelloch, R., and Kimble, J. (1996). Roles of the RAM and ANK domains in signaling by the C. elegans GLP-1 receptor. EMBO J. *15*, 7002–7012.

Shiau, A.K., Barstad, D., Loria, P.M., Cheng, L., Kushner, P.J., Agard, D.A., and Greene, G.L. (1998). The structural basis of estrogen receptor/coactivator recognition and the antagonism of this interaction by tamoxifen. Cell *95*, 927–937.

Struhl, G., and Grenwald, I. (1999). Presenilin is required for activity and nuclear access of Notch in Drosophila. Nature *398*, 522–525.

Tani, S., Kurooka, H., Aoki, T., Hashimoto, N., and Honjo, T. (2001). The N- and C-terminal regions of RBP-J interact with the ankyrin repeats of Notch1 RAMIC to activate transcription. Nucleic Acids Res. *29*, 1373–1380.

Tun, T., Hamaguchi, Y., Matsunami, N., Furukawa, T., Honjo, T., and Kawaichi, M. (1994). Recognition sequence of a highly conserved DNA binding protein RBP-J kappa. Nucleic Acids Res. *22*, 965–971.

Uyttendaele, H., Marazzi, G., Wu, G., Yan, Q., Sassoon, D., and Kitajewski, J. (1996). Notch4/int-3, a mammary proto-oncogene, is an endothelial cell-specific mammalian Notch gene. Development *122*, 2251–2259.

Vagin, A., and Teplyakov, A. (1997). MOLREP: an automated program for molecular replacement. J. Appl. Crystallogr. *30*, 1022–1025.

Vagin, A.A., Steiner, R.A., Lebedev, A.A., Potterton, L., McNicholas, S., Long, F., and Murshudov, G.N. (2004). REFMAC5 dictionary: organization of prior chemical knowledge and guidelines for its use. Acta Crystallogr. D Biol. Crystallogr. *60*, 2184–2195.

van Es, J.H., van Gijn, M.E., Riccio, O., van den Born, M., Vooijs, M., Begthel, H., Cozijnsen, M., Robine, S., Winton, D.J., Radtke, F., and Clevers, H. (2005). Notch/gamma-secretase inhibition turns proliferative cells in intestinal crypts and adenomas into goblet cells. Nature *435*, 959–963.

Wallberg, A.E., Pedersen, K., Lendahl, U., and Roeder, R.G. (2002). p300 and PCAF act cooperatively to mediate transcriptional activation from chromatin templates by notch intracellular domains in vitro. Mol. Cell. Biol. *22*, 7812–7819.

Weng, A.P., Nam, Y., Wolfe, M.S., Pear, W.S., Griffin, J.D., Blacklow, S.C., and Aster, J.C. (2003). Growth suppression of pre-T acute lymphoblastic leukemia cells by inhibition of notch signaling. Mol. Cell. Biol. *23*, 655–664.

Weng, A.P., Ferrando, A.A., Lee, W., Morris, J.P.T., Silverman, L.B., Sanchez-Irizarry, C., Blacklow, S.C., Look, A.T., and Aster, J.C. (2004). Activating mutations of NOTCH1 in human T cell acute lymphoblastic leukemia. Science *306*, 269–271.

Wu, L., Aster, J.C., Blacklow, S.C., Lake, R., Artavanis-Tsakonas, S., and Griffin, J.D. (2000). MAML1, a human homologue of Drosophila mastermind, is a transcriptional coactivator for NOTCH receptors. Nat. Genet. *26*, 484–489.

Wu, L., Sun, T., Kobayashi, K., Gao, P., and Griffin, J.D. (2002). Identification of a family of mastermind-like transcriptional coactivators for mammalian notch receptors. Mol. Cell. Biol. *22*, 7688–7700.

Ye, Y., Lukinova, N., and Fortini, M.E. (1999). Neurogenic phenotypes and altered Notch processing in Drosophila Presenilin mutants. Nature *398*, 525–529.

Zweifel, M.E., Leahy, D.J., Hughson, F.M., and Barrick, D. (2003). Structure and stability of the ankyrin domain of the Drosophila Notch receptor. Protein Sci. *12*, 2622–2632.

Accession Numbers

Coordinates for the blunt-ended DNA complex and for the ankyrin repeat domain of Notch1 have been deposited in the Protein Data Bank under accession codes 2F8X and 2F8Y, respectively.